Analysis of Small-Scale Wind Turbine Blades for Optimal Power Generation: A CFD-BEMT Study

Jasson Fernandez Gurgel[1], Pedro Lucas Barros Martins[1], Carla Freitas de Andrade[1], Francisco Olimpio Moura Carneiro[2], Francisco Nivaldo Aguiar Freire[1], Felipe Cordeiro de Sousa[1]

[1] Federal University of Ceará, Fortaleza (Brazil))

[2] University of International Integration of Afro-Brazilian Lusophone, Redenção (Brazil)

Abstract

This study numerically compares the aerodynamic performance of blades for horizontal axis wind turbines (HAWT) with a rotor diameter of 0.5 m, aiming to maximize the generated power. Two blade geometries were evaluated, based on the GOE 770 and AH 93-W-215 profiles, selected due to their accessibility for working with additive manufacturing techniques in prototype fabrication. In this context, the chord and twist distributions were defined using Blade Element Momentum Theory (BEMT) for fixed pitch operation. The simulations were conducted in the open-source software OpenFOAM, in transient mode, using a RANS approach for turbulence modeling. The flow velocity was set at 5 m s^{-1}, a wind speed characteristic of the region in which the study was developed, and the rotor rotation condition was imposed based on experimental data obtained in a wind tunnel, ensuring the representativeness of actual operating conditions. The main metric used to compare the performance of the wind turbines was the average torque of the last 10º simulated in each set. Finally, the results indicate that the blade based on the GOE 770 profile has a higher power generation capacity than the one based on the AH 93-W-215 profile under the tested conditions, highlighting the joint importance of aerodynamic profile selection, prototype manufacturability, and transient numerical modeling in the optimization of small-scale wind turbines.

Keywords: Renewable Energy, Wind Energy, HAWT, BEMT, CFD, OpenFOAM, RANS.

1. Introduction

The transition to low-carbon energy matrices has driven the development of wind technologies on multiple scales, with an emphasis on small-scale applications for distributed generation, rural electrification, urban use, and integration with hybrid systems. In this context, small-scale horizontal axis wind turbines (HAWT) present specific design challenges due to low Reynolds numbers, greater susceptibility to atmospheric flow conditions, and prototype manufacturing constraints. Aerodynamic optimization of the blades, combined with manufacturing feasibility and reliable numerical modeling, is crucial to maximize power extraction and ensure robust performance under realistic operating conditions (Burton et al., 2001).

Technical literature has consolidated theoretical and methodological bases for the aerodynamic design of rotors, in which Blade Element Momentum Theory (BEMT) remains the basic tool for defining radial chord and twist distributions, especially in fixed pitch configurations. Recent studies indicate that careful choices of aerodynamic profiles, combined with strategies for optimizing and linearizing twist and chord compatible with manufacturing limitations, and the use of tip and root loss corrections, can significantly increase the power coefficient on a small scale (Hansen, 2008). At the same time, advances in the field of Computational Fluid Dynamics (CFD) with turbulence analysis via numerical models, such as RANS, in transient conditions, have made it possible to capture three-dimensional aerodynamic effects, separation, and dynamic stall with greater accuracy, provided that they are accompanied by good practices in mesh independence, choice of turbulence models, and representative boundary conditions (Bai et al., 2016).

Within this context, the present study aims to numerically compare the aerodynamic performance of blades for a HAWT with a rotor diameter of 0.5 m, with a view to maximizing power in fixed pitch operation. Two blade geometries are evaluated in this work, based on the GOE 770 and AH 93 W 215 profiles, chosen both for their

10.18086/swc.2025.05.01 Available at http://proceedings.ises.org

aerodynamic potential at low Reynolds numbers and for their accessibility for additive manufacturing of prototypes. The chord and twist distributions are determined by BEMT, ensuring consistency with established preliminary design practices for small-scale rotors. For numerical analysis, OpenFOAM is used in transient mode, with RANS turbulence modeling, aiming to capture non-stationary phenomena relevant to torque generation; the flow velocity is set at 5 m/s, and the rotor rotation is imposed based on experimental data obtained in a wind tunnel, ensuring representativeness of operating conditions and strengthening the link between simulation and testing. Aerodynamic performance is compared based on average torque, a metric directly associated with extracted power and sensitive to differences in profile and geometric distribution (Manwell et al., 2002).

2. Methodology

The approach combines the development of a preliminary design using Blade Element Momentum Theory (BEMT), CAD modeling compatible with additive manufacturing, and transient Computational Fluid Dynamics (CFD) simulations in OpenFOAM with RANS turbulence modeling, under representative operating conditions obtained in a wind tunnel.

The selection of aerodynamic profiles fell on the GOE 770 and AH 93-W-215 profiles, chosen for their performance potential at low Reynolds numbers, wide availability of geometric coordinates, and compatibility with additive manufacturing techniques, providing sufficient thickness in the tip region for internal reinforcement with carbon fiber filament. The manufacturing criteria considered the geometric integrity of the leading and trailing edges, relative thicknesses appropriate to the scale and structural strength of the prototype, as well as the need for smoothing coordinates to ensure surface continuity in the CAD stage and suitability for geometry in mesh generation. These aspects ensure that the simulated geometries can be prototyped without significant deviations from the theoretical design. The GOE 770 and AH 93-W215 aerodynamic profiles are shown in Figures 1 and 2, respectively.

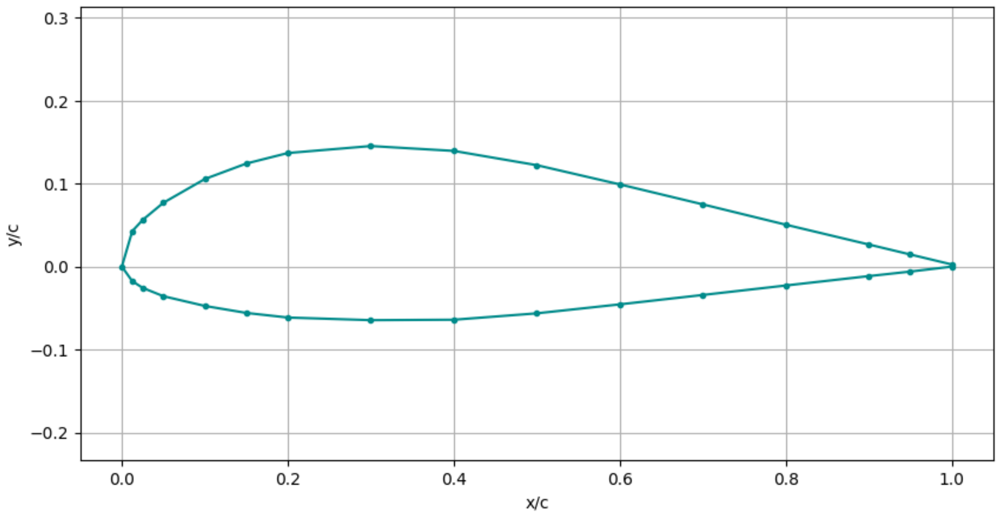

Figure 1: Coordinates of the GOE 770 aerodynamic profile with unit chord length.

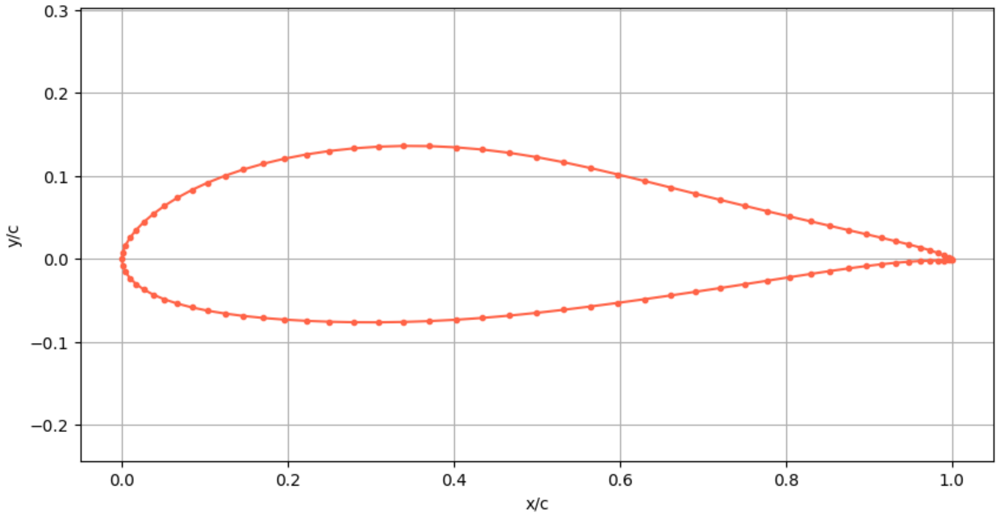

Figure 2: Coordinates of the AH 93-W-215 aerodynamic profile with unit chord length.

The operating conditions for each simulation were defined to reflect a representative experimental scenario: rotor diameter D = 0.5 m (radius R = 0.25 m), fixed pitch operation, flow velocity U_∞ = 5 m s^{-1} and rotor rotation Ω imposed based on data obtained in a wind tunnel. This rotation imposition, derived from measurements under similar conditions, aims to reinforce the operational representativeness of the numerical simulations. The number of blades and the corresponding tip speed ratio (λ) were determined in order to ensure the manufacturability of the prototype and maximum power extraction from the experimental assembly, allowing direct evaluation of the average torque as the main comparison metric. The fluid properties (density ρ, dynamic viscosity μ, and temperature T) followed the environmental conditions of the tunnel in which the tests with the prototypes were performed, ensuring consistency between testing and simulation. The operating conditions of the rotors and air in the wind tunnel tests are provided in Tables 1 and 2.

Table 1: Air properties for numerical simulation.

Parameter	Symbol	Value
Density	ρ	1.164734 kg m^{-3}
Dynamic viscosity	μ	0.000019 Pa s
Temperature	T	30 °C

Table 2: Rotations observed in wind tunnel tests with U∞ = 5 m s^{-1}.

Wind Blade	Angular Velocity (Ω)
GOE 770	139.49 rad s^{-1}
AH 93-W-215	108.18 rad s^{-1}

The preliminary design of the blades was conducted by BEMT, assuming constant tip speed ratio operation, adopting the optimal axial induction factor (a = 1/3), a choice based on the theoretical Betz limit, which establishes the maximum fraction of wind kinetic energy that can be converted into mechanical power by an ideal rotor, a condition that maximizes the power coefficient (C_p) of the rotor. This behavior is evident in Figure 3, which shows the C_p versus λ (Tip Speed Ratio) graph, in which it can be observed that the maximum C_p value occurs for a tip speed ratio close to 6, and the consistent derivation of the tangential induction factor along the radius.

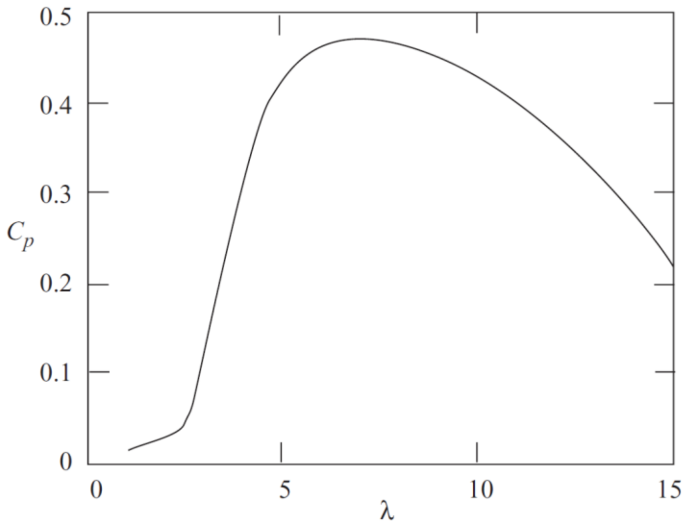

Figure 3: Power coefficient (Cp) vs Tip Speed Ratio (Hau, 2006).

For each radial position, The relative flow velocity and flow angle were determined, from which the local twist was defined as the difference between the flow angle (Φ) and the optimum angle of attack (α) of the airfoil. The chord distribution was calculated considering the number of blades, lift coefficient (C_L) at the optimum point, and the radial variation of the induction factors, ensuring consistency with fixed pitch operation. Figure 4 shows the force and velocity components acting on each blade element.

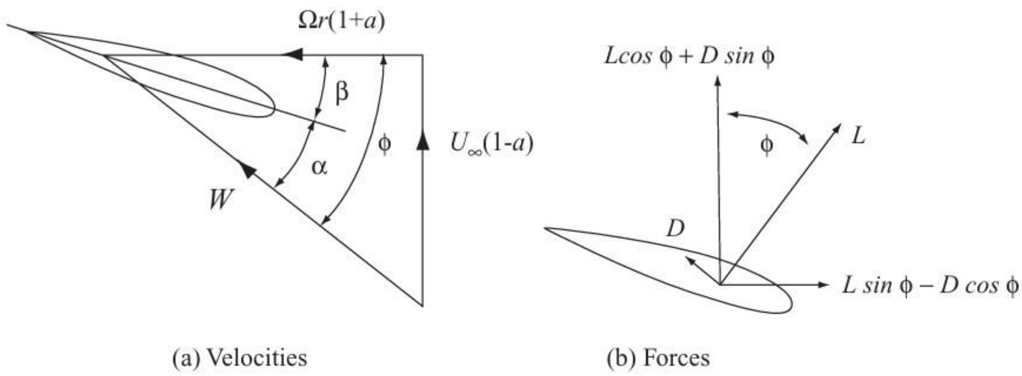

Figure 4: Forces and velocities acting on the radial element (Burton et al., 2001).

The axial induction factor is set at its optimum value, as predicted by the Betz limit:

$$a = \frac{1}{3} \qquad \text{(eq. 1)}$$

The tangential induction factor is then calculated by:

$$a' = \frac{a\,(1-a)}{\lambda^2 \mu^2} \qquad \text{(eq. 2)}$$

Where:

$$\mu = \frac{r}{R} \qquad \text{(eq. 4)}$$

And r is the local radius and R is the total radius of the blade. The angular velocity of the rotor is given by:

$$\Omega = \frac{\lambda U_\infty}{R}$$ (eq. 4

Where U_∞ is the upstream wind speed. The relative speed to the blade element is:

$$W = \sqrt{{U_\infty}^2(1-a)^2 + [\Omega r(1+a^1)]^2}$$ (eq. 5)

The relative flow angle is calculated by:

$$\phi = arctan\left(\frac{1-a}{\lambda\mu(1+a')}\right)$$ (eq. 6)

The distribution of chord along the paddle, considering the simplified method, is given by:

$$c(\mu) = \frac{8\pi R\lambda\mu^2 a'}{NC_L\sqrt{(1-a)^2+[\lambda\mu(1+a')]^2}}$$ (eq. 7)

Where N is the number of blades and C_L is the lift coefficient for the optimum angle of attack. Finally, the twist distribution is obtained by:

$$\theta(\mu) = \phi - \alpha$$ (eq. 8)

where α is the optimum angle of attack (Burton et al., 2001).

With this information, the input parameters for each wind turbine blade were defined for modeling, as shown in Tables 3 and 4, following the optimized design methodology proposed by BEMT.

Table 3: Input parameters for applying the BEMT method to the GOE 770 profile.

Parameter	Symbol	Value
Axial induction factor	a	1/3
Tip speed ratio	λ	6
Optimal angle of attack	α	6.00 º
Optimal lift coefficient	C_L	0.9571
Blade radius	R	0.25 m
Number of blades	N	2
Number of sections	n	19

Table 4: Input parameters for applying the BEMT method to the AH 93-W-215 profile.

Parameter	Symbol	Value
Axial induction factor	a	1/3
Tip speed ratio	λ	6
Optimal angle of attack	α	6.25 º
Optimal lift coefficient	C_L	0.7804
Blade radius	R	0.25 m
Number of blades	N	2

Number of sections	n	19

The results obtained from modeling the wind turbine blades, GOE 770 and AH 93-W-215, using the BEMT optimal design equations are presented in Tables 5 and 6, respectively.

Table 5: Results obtained for the geometric modeling of the GOE 770 profile via BEMT.

Section	r (m)	μ	Φ (º)	c (m)	Twist (º)	a	a'
1	0.0250	0.10	34.49	0.1033	28.49	0.333	0.6173
2	0.0375	0.15	30.17	0.0916	24.17	0.333	0.2743
3	0.0500	0.20	25.70	0.0791	19.70	0.333	0.1543
4	0.0625	0.25	22.02	0.0684	16.02	0.333	0.0988
5	0.0750	0.30	19.12	0.0597	13.12	0.333	0.0686
6	0.0875	0.35	16.82	0.0528	10.82	0.333	0.0504
7	0.1000	0.40	14.97	0.0471	8.97	0.333	0.0386
8	0.1125	0.45	13.47	0.0425	7.47	0.333	0.0305
9	0.1250	0.50	12.24	0.0386	6.24	0.333	0.0247
10	0.1375	0.55	11.20	0.0354	5.20	0.333	0.0204
11	0.1500	0.60	10.32	0.0327	4.32	0.333	0.0171
12	0.1625	0.65	9.56	0.0303	3.56	0.333	0.0146
13	0.1750	0.70	8.91	0.0282	2.91	0.333	0.0126
14	0.1875	0.75	8.34	0.0264	2.34	0.333	0.0110
15	0.2000	0.80	7.83	0.0249	1.83	0.333	0.0096
16	0.2125	0.85	7.39	0.0234	1.39	0.333	0.0085
17	0.2250	0.90	6.99	0.0222	0.99	0.333	0.0076
18	0.2375	0.95	6.63	0.0210	0.63	0.333	0.0068
19	0.2500	1.00	6.30	0.0200	0.30	0.333	0.0062

Table 6: Results obtained for the geometric modeling of the AH 93-W-215 profile via BEMT.

Section	r (m)	μ	Φ (º)	c (m)	Twist (º)	a	a'
1	0.0250	0.10	34.49	0.1266	28.24	0.333	0.6173
2	0.0375	0.15	30.17	0.1124	23.92	0.333	0.2743
3	0.0500	0.20	25.70	0.0970	19.45	0.333	0.1543
4	0.0625	0.25	22.02	0.0839	15.77	0.333	0.0988
5	0.0750	0.30	19.12	0.0732	12.87	0.333	0.0686
6	0.0875	0.35	16.82	0.0647	10.57	0.333	0.0504

7	0.1000	0.40	14.97	0.0578	8.72	0.333	0.0386
8	0.1125	0.45	13.47	0.0521	7.22	0.333	0.0305
9	0.1250	0.50	12.24	0.0474	5.99	0.333	0.0247
10	0.1375	0.55	11.20	0.0434	4.95	0.333	0.0204
11	0.1500	0.60	10.32	0.0401	4.07	0.333	0.0171
12	0.1625	0.65	9.56	0.0372	3.31	0.333	0.0146
13	0.1750	0.70	8.91	0.0346	2.66	0.333	0.0126
14	0.1875	0.75	8.34	0.0324	2.09	0.333	0.0110
15	0.2000	0.80	7.83	0.0305	1.58	0.333	0.0096
16	0.2125	0.85	7.39	0.0287	1.14	0.333	0.0085
17	0.2250	0.90	6.99	0.0272	0.74	0.333	0.0076
18	0.2375	0.95	6.63	0.0258	0.38	0.333	0.0068
19	0.2500	1.00	6.30	0.0245	0.05	0.333	0.0062

The CAD modeling of the two geometries was performed by interpolating sections with GOE 770 and AH 93-W-215 profiles, incorporating radial twist θ(r) and chord fro each section. Surface continuity, minimum thickness, and smooth transition checks were performed in the root region. For the CFD simulation, a domain was adopted consisting of a rotating internal region involving the rotor and a stationary external region, coupled by an AMI (Arbitrary Mesh Interface) (Carneiro, 2019). The dimensions of the domain were established to minimize blocking and recirculation effects: the upstream and downstream extension and radius of the domain were defined with multiples of the diameter compatible with the literature and the target computational cost, ensuring that the wake and tip vortices developed without interference from the boundaries (Carneiro, 2020).

The mesh generation aimed to balance computational cost and efficiency, with an emphasis on prismatic layers near the blade surfaces for adequate boundary layer resolution, and localized refinements on the upper surface, lower surface, edges, and regions of intense vorticity (tip and root), as well as the vicinity of the AMI interface (Carneiro, 2011) . The wall treatment was configured for the k-ω SST model, adopting consistency between cases regarding the y+ target (resolution of the viscous sublayer with $y+ \lesssim 1$ or consistent use of wall functions with y+ between 30 and 100) (Thé et al., 2017).

Table 7: Number of computational mesh elements for each set.

Wind Blade	Number of elements in the computational mesh
GOE 770	6418789
AH 93-W-215	4649843

The simulations were conducted in OpenFOAM in transient mode, with turbulence modeling via RANS k-ω SST. Pressure-velocity coupling was performed via the PIMPLE algorithm, using second-order numerical schemes (limited when necessary) for convective and diffusive terms (Lee et al., 2006). The time step Δt was chosen to maintain the Courant number $Co \leq 1$ (preferably ≤ 0.5), and the sensitivity of the average torque to variations in Δt was verified. The boundary conditions included: inlet with velocity $U = 5$ m/s and specification of turbulence intensity and scale consistent with tunnel conditions; outlet with reference pressure condition; blade walls with no-slip condition and compatible wall functions; and cyclicAMI interface between rotating and stationary regions. The rotation of the internal region was imposed with Ω corresponding to the experimental measurements, ensuring the representativeness of the actual operating conditions. The total simulation time covered a single revolution of the rotors, discarding the initial transient regime and integrating the torque over periodic windows to obtain the average value.

The boundary conditions used in model k-ω SST for each region of the computational model are listed in Table 8.

Table 8: Boundary conditions applied to model k-ω SST.

Region	Boundary Condition			
	Velocity	Pressure	k	ω
Inlet	5 m s^{-1}	Zero Gradient	0.634 m^2 s^{-2}	41.248 s^{-1}
Outlet	Zero Gradient	0 Pa	Zero Gradient	Zero Gradient
Walls	Zero Gradient	Zero Gradient	Zero Gradient	Zero Gradient
Rotating region	Table 2	Zero Gradient	Zero Gradient	Zero Gradient

Monitoring and post-processing covered instantaneous torque on the shaft and its average value per revolution after establishing periodic or quasi-stationary conditions. The convergence of each simulation was evaluated by the behavior of the residuals and the periodicity of the torque over the simulated time.

The comparison between geometries considered as primary metric the average torque in the condition $U\infty = 5$ m/s and Ω imposed. Secondary metrics included the smoothness of the torque signal (azimuth variations), the adequate resolution of the pressure field at certain angular positions, and the sensitivity to small variations of Ω, when applicable.

The integration of computational simulations with experimental data was achieved by imposing Ω and parameterizing the turbulence levels at the inlet, reflecting the wind tunnel conditions. Although this is not a strict validation study, consistency between simulation and testing was sought. Finally, quality controls were established to ensure consistency between the two compared cases: use of the same numerical tools (solver, schemes, and boundary conditions), equivalent mesh strategy with compatible y+ criteria, time step studies, and identical post-processing and metric calculation procedures.

3. Results and Discussion

The results of the computational simulations indicate marked differences between the performance of the wind turbine blade profiles evaluated, GOE 770 and AH 93-W-215, when analyzing the moment as a function of the azimuth angle and the associated power. Figure 5 shows the Moment vs. Azimuth Angle chart.

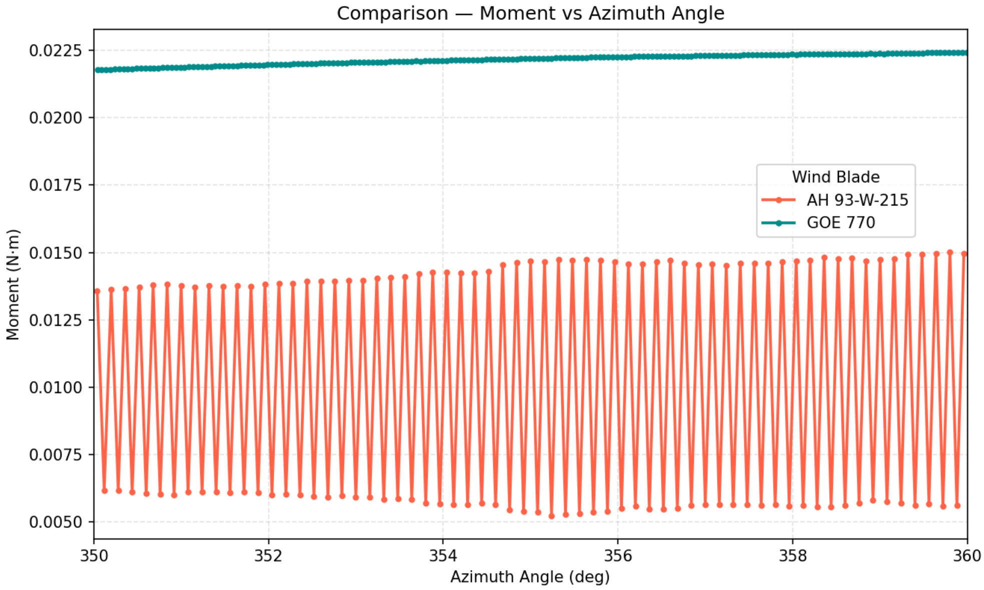

Figure 5: Comparison chart of Moment vs Azimuth Angle of GOE 770 and AH 93-W-215 wind blades.

The values shown in Table 9 indicate that, under stable operating conditions, the wind blade using the GOE 770 profile delivers approximately 2.2 times more torque and about 2.8 times more power than the AH 93-W-215 under the operating conditions considered. This advantage is in line with the instantaneous behavior observed: the wind turbine blade with the GOE 770 airfoil exhibits a virtually flat torque signal, with a slight tendency to increase as the azimuth angle advances, suggesting a more uniform pressure distribution and less sensitivity to local variations in the angle of attack. The wind turbine blade with the AH 93-W-215 airfoil, on the other hand, exhibits pronounced oscillations over a single revolution, characterizing a more pulsating loading and, potentially, a less uniform pressure distribution..

Table 9: Average power and moment results for the last 10º for the simulated wind blades.

Wind Blade	Moment	Power
GOE 770	0.0222 N m	3.0976 W
AH 93-W-215	0.0101 N m	1.0895 W

The interpretation of these high oscillations in the case of AH 93-W-215 most likely points to limitations of the mesh used in adequately resolving the pressure field, especially in regions with steep gradients near the leading edge and trailing edge, as well as in areas subject to flow separation. Insufficient discretization or geometric quality that is less than ideal can introduce numerical truncation and dispersion/dissipation errors, amplifying fluctuations in surface loading and converting smooth physical phenomena into numerical torque oscillations. In addition, the computational mesh for AH 93-W-215 (approximately 4.65 million elements) is notably coarser than that for GOE 770 (about 6.42 million elements), implying roughly 38% fewer cells available to capture boundary-layer gradients, tip/root vortices, and pressure recoveries. This lower spatial resolution can exacerbate under-resolution of separation onset and reattachment, leading to spurious high-frequency torque ripple; conversely, the denser GOE 770 mesh likely contributes to the smoother torque signal observed by better resolving near-wall shear and adverse pressure gradients. It is important to note that, despite this oscillatory behavior, both simulations converged according to the criteria adopted, with stabilization of the average torque per revolution and consistent reduction of residuals, indicating numerically consistent solutions. Thus, the dominant effect seems to be linked to the spatial fidelity of the mesh, rather than the absence of iterative or transient convergence.

In summary, the results position GOE 770 as the preferred option for the scenario studied, combining higher torque and power output with more stable loading across the azimuth. Confirmation of the behavior of AH 93-W-215 requires repeating the simulations with higher resolution and better quality meshes to unequivocally separate the numerical effects from the physical phenomena, thus ensuring a fair and robust assessment of its aerodynamic performance.

4. Conclusion

The numerical analysis conducted in this study allowed for a comparison, under representative operating conditions, of the aerodynamic performance of two blade geometries for a small horizontal axis wind turbine (D = 0.5 m), designed using BEMT and simulated in transient mode with the k-ω SST model in OpenFOAM. The results indicate that the blade based on the GOE 770 profile performs better than the blade based on the AH 93-W-215 profile, as expressed by higher average torque and higher power extracted under wind conditions of 5 m/s and rotation imposed from wind tunnel data. In addition to the average advantage, GOE 770 showed a more stable torque signal throughout the azimuth angle advance, a desirable feature from an energy and structural point of view as it reduces the pulsating nature of the load and its potential implications for vibration and fatigue. Although the AH 93-W-215 case exhibited marked oscillations in instantaneous torque, the simulations of both profiles converged according to the criteria adopted (residuals and stabilization of average torque per revolution), suggesting that the observed oscillations stem mainly from mesh limitations in pressure field resolution, rather than from a lack of numerical convergence. Thus, within the scope evaluated, GOE 770 is consolidated as the preferred alternative for maximizing power in fixed-pitch operation, reconciling aerodynamic performance and additive manufacturing feasibility. However, it is recommended that a mesh independence study and localized refinement in regions of pressure gradients of the AH 93-W-215 be carried out, as well as complementary analyses of sensitivity to time step and turbulence parameters, to unequivocally isolate the numerical effects of physical phenomena and consolidate the robustness of the conclusions presented here.

5. Acknowledgments

The authors would like to thank FUNCAP - Fundação Cearense de Apoio ao Desenvolvimento Científico e Tecnológico (Research and Innovation Network on Renewable Energy, Rede VERDES, grant 07548003/2023), CNPq – Conselho Nacional de Pesquisa, Universal - Proc. No. 408431/2023-7 and Bolsa de Produtividade em Pesquisa, CNPq - Proc. No. 307096/2021-1 Also, this study was financed in part by the Coordenação de Aperfeiçoamento de Pessoal de Nível Superior - Brasil (CAPES)- Finance Code 001 and Conselho Nacional de Desenvolvimento Científico e Tecnológico - Brasil (CNPq) - process 301227/2025-0.

6. References

Bai, C.-J., Wang, W.-C., 2016. Review of computational and experimental approaches to analysis of aerodynamic performance in horizontal-axis wind turbines (HAWTs). Renewable and Sustainable Energy Reviews, 63, 506–519.

Burton, T., Shape, D., Jenkins, N., Bossanyi, E., 2001. Wind energy handbook, John Wiley & Sons Ltd.

Carneiro, F. O. M., 2019. Application and analysis of the moving mesh algorithm AMI in a small scale HAWT: Validation with field test's results against the frozen rotor approach, Energy, v. 171, p. 819-829.

Carneiro, F. O. M., 2011. Levantamento de curvas de eficiência de aerogeradores de 3m de diâmetro utilizando modelos de turbulência RANS de uma e duas equações comparação experimental, Master's Thesis, Universidade Federal do Ceará.

Carneiro, F. O. M., 2020. Estudo comparativo do levantamento da curva de eficiência de um aerogerador de pequeno porte utilizando OpenFOAM com diferentes abordagens numéricas e dados experimentais, PhD Thesis, Universidade Estadual de Campinas.

Chehouri, A., Younes, R., Ilinca, A., Perron, J., 2015. Review of performance optimization techniques applied to wind turbines. Applied Energy, 142, 361–388.

Costa Rocha, C., Silveira-Neto, A., Catalano, F.M., 2014. k–ω SST (shear stress transport) turbulence model calibration: A case study on a small-scale horizontal axis wind turbine. Renewable Energy, 75, 616–627, 2014.

Dai, Y., Guo, P., Liang, X., Liu, L., 2015. Optimized linearization of chord and twist angle profiles for fixedpitch fixed-speed wind turbine blades. Energy Conversion and Management, 101, 387–396.

Lee, M.-H., Shiah, Y.-C., Bai, C.-J., 2016. Experiments and numerical simulations of the rotor-blade performance for a small-scale horizontal axis wind turbine. Journal of Wind Engineering and Industrial Aerodynamics, 149, 17–29. Hau, E., Wind Turbines, Springer, Second Edition.

Liu, Y., Qiu, Y., Dong, X., Chen, Y., 2013. A method for preliminary rotor design – Part 2: Wind turbine optimization with radial independence. Renewable Energy, 60, 271–282.

Manwell, J. F, McGowan, J. G., Rogers, A. L., 2002. Wind Energy Explained – Theory, Design and Application, John Wiley & Sons Ltd.

Minh, H.T., Vo, T.V., Hoang, A.H., 2023. Predicting aerodynamic performance of Savonius wind turbine: Experimental and numerical study. Renewable Energy, 202, 42–58.

Thé, J., Yu, H., 2017. A critical review on the simulations of wind turbine aerodynamics focusing on hybrid RANS–LES methods. Energy, 138, 257–289.